Electronic Supplementary Material (ESI) for Catalysis Science & Technology.

Supporting information

Highly dispersed Rh single atoms over graphitic carbon nitride as a robust catalyst for the hydroformylation reaction

Lole Jurado,[a] Jerome Esvan,[b] Ligia A. Luque-Álvarez,[c] Luis F. Bobadilla,[c] José A. Odriozola,[c] Sergio Posada-Pérez,[d] Albert Poater,[d] Aleix Comas-Vives,[e, f] and M. Rosa Axet [a]*

[a] CNRS, LCC (Laboratoire de Chimie de Coordination), Université de Toulouse, UPS, INPT, 205 route de Narbonne, F-31077 Toulouse Cedex 4, France

[b] CIRIMAT, Université de Toulouse, CNRS-INPT-UPS, 4 Allée Emile Monso, 31030 Toulouse, France

[c] Departamento de Química Inorgánica e Instituto de Ciencia de Materiales de Sevilla, Centro Mixto CSIC-Universidad de Sevilla, Av. Américo Vespucio 49, 41092 Sevilla (Spain)

[d] Institut de Química Computacional i Catàlisi and Departament de Química, Universitat de Girona, c/ Maria Aurèlia Capmany 69, 17003 Girona, Catalonia, Spain

[e] Institute of Materials Chemistry, TU Wien, 1060 Vienna, Austria

[f] Departament de Química, Universitat Autònoma de Barcelona, 08193 Cerdanyola del Vallès, Catalonia, Spain

*Corresponding author: M. Rosa Axet (rosa.axet@lcc-toulouse.fr)

General Methods. Most of the operations were performed under argon atmosphere by using standard Schlenk lines or in an MBraun glovebox. All solvents were previously purified by standard methods or using an MBraun SPS-800 solvent purification system. Rhodium chloride trihydratate ($RhCl_3$ 3 H_2O) was purchased from Johnson and Matthey, allylmagnesium chloride, tetrahydrofuran (THF), pentane, styrene and octane from Sigma-Aldrich, dyciandiamide 99% (DCAD), 2-phenylpropionaldehyde, 3-phenylpropionaldehyde, 2-phenyl-1-propanol, 3-phenyl-1-propanol, ethylbenzene and ethylcyclohexane from Alfa Aesar and CO and H_2 from Air Liquid. All these reactants were used as received. Metal content was established by inductively coupled plasma optical emission spectroscopy (ICP-OES) performed in a Thermo Scientific ICAP 6300 instrument. The elemental composition (C, N and H content) of the synthesized materials was determined by elemental analysis using a PERKIN ELMER 2400 serie II CHNS/O Elemental Analyser Liquid NMR measurements were performed on a Bruker Avance 300 or 400 instrument. Attenuated total reflection infrared (ATR-IR) spectra were recorded on a Perkin-Elmer GX2000 spectrometer available in a glovebox, in the range 4000-400 cm^{-1}. Transmission electron microscopy (TEM) and high resolution transmission electron microscopy (HRTEM) analyses were performed at the "Centre de microcaracterisation Raimond Castaing, UMS 3623, Toulouse" by using a JEOL JEM 1011 CXT electron microscope operating at 100 kV with a point resolution of 4.5 Å or a JEOL JEM 1400 operating at 120 kV with a point resolution of 2.0 Å. High resolution analyses were conducted using a JEOL JEM-ARM200F Cold FEG operating at 200 kV with a point resolution of >1.9 Å. The crystalline phases of the materials were identified by X-ray diffraction (XRD) on a Rigaku Miniflex 600 diffractometer equipped with a D/teX ultra 1D silicon strip detector and monochromatic Cu K_α radiation (1.5418 Å). All diffractograms were recorded over a 2θ range of 5-60° using a step size of 0.050° and step time of 1s. The crystallite size of the support ($d_{support}$) was estimated by Debye-Scherrer equation using the most intense peak placed at 2θ ~27 ° linked to the (002) reflection. In addition; the size of the tri-s-triazine ring as well as the interplanar distance were estimated through the Bragg's law considering respectively the peaks at 2θ ~13°, related to (100) reflection and, at 2θ ~27 ° related to (002) reflection. X-ray photoelectron spectroscopy (XPS) experiments under ultra high vacuum (UHV) were performed with Thermo Scientific K-Alpha apparatus using a monochromatised Al Kα (EAl Kα = 1486.6 eV) X-ray source. The X-ray spot size was about 400 µm. The Pass energy was fixed at 30 eV with a step of 0.1 eV for core levels and 160 eV for surveys (step 1eV). The spectrometer energy calibration was done using the Au 4f7/2 (83.9 ± 0.1 eV) and Cu 2p3/2 (932.8 ± 0.1 eV) photoelectron lines. XPS spectra were recorded in direct mode N (Ec) and the background signal was removed using the Shirley method. The flood Gun was used to neutralize charge effects on the top surface. Thermogravimetric analysis (TGA) were performed on a TGA/DSC 3+ Mettler Toledo. Samples were heated up to 1073 K under N_2 flow (50 mL· min^{-1}) using a heating ramp of 10 K·min^{-1} for fresh materials, whereas a heating ramp of 2 K·min^{-1} was used for the spent materials. The textural properties such as specific surface area (SSA) and pore volume (V_{pore}) were determined by N_2 physisorption at 77 K using the Brunauer-Emmet-Teller (BET) method on a Micromeritics ASAP 2020 plus. Prior the analysis, samples were outgassed at 523 K for 4 h in order to remove the moisture adsorbed on the surface and inside the pores. *In situ* DRIFTS measurements were performed using a high temperature environmental reaction chamber supported in a Praying Mantis (*Harrick*) DRIFTS optical system with ZnSe windows. The spectra were collected using a Thermo Nicolet iS50 FTIR spectrometer equipped with a liquid nitrogen cooled MCT detector at 4 cm^{-1} resolution and average of 128 scans. About 50 mg of catalyst finely ground was loaded in the cell for each measurement. CO adsorption experiments were performed by feeding a flow rate of 50 mL· min^{-1} of a mixture of 2% CO/Ar into the IR cell heated at 50 °C during 20 min. Afterwards, the sample was purged with a flow of 50 mL min^{-1} of pure Ar during 5 min. In both adsorption and purge measurements spectra were recorded in continuous mode. A four-way valve was installed to allow switching between both gas mixture and gas purging. The gas flow rates were controlled by mass-flow controllers from AALBORG appropriately calibrated. Quantitative analyses of the catalytic reaction mixtures were performed via gas chromatography (GC) analyses using internal standard technique and solutions of commercially available products. GC analyses were performed on a SHIMADZU GC-2010 equipped with a ZEBRON ZB-5ms capillary column (30 m x 0.25 mm x 0.25µm). The method used for styrene hydroformylation reaction mixture analyses consists on: carrier gas flow, He, 1.25 ml/min; injector temperature, 250 °C; detector (FID) temperature, 250 °C; oven program, 50 °C (hold 3 min) to 240 °C at 10 °C/min (hold 10 min) for a total run time of 22 min; retention time: octane, 4.4 min; styrene, 6.3 min; ethylcyclohexane, 5.1 min; ethylbenzene, 5.6 min; 2-phenylpropionaldehyde, 10.3 min; 3-phenylpropionaldehyde, 11.3 min; 2-phenyl-1-propanol, 11.4 min; and 3-phenyl-1-propanol, 12.3 min.

Computational details. Periodic density functional calculations (DFT) were carried out using the Vienna *Ab initio* Simulation Package (VASP) code.[1] The PBE exchange-correlation (xc) functional[2] was used for the description C_3N_4 surfaces. The semi-empirical method of Grimme (D3) to describe the dispersion correction effects.[3] The ionic relaxation convergence was smaller than 0.01 eV $Å^{-1}$ and the electronic relaxation was considered converged when the total energy in subsequent iterations varied less than 10^{-5} eV. The effects caused by the core electrons on the valence ones were described through the projected augmented wave (PAW) method of Blöch[4] as implemented by Kresse and Joubert.[5] The reciprocal space was described by means of a 3×3×1 Monkhorst-Pack scheme.[6] The slab models contained three fully relaxed atomic layers obtained from the initial bulk structure (Materials Projects Database, id: mp-971684.[7] Each layer contains 24 C and 32 N atoms. We evaluated the stability of the Rh atom deposited on the top-most exposed layer and intercalated between layers. The adsorption of CO, H, and ethylene have been carried out on top of the surface and Rh atom. All the minima structures have been fully characterized via pertinent frequency analysis of the modes related to the adsorbate within the harmonic approximation. It has been obtained by construction and diagonalization of the Hessian matrix by individual displacements of 0.03 Å in each cell direction and including all the Rh-cluster atoms, not the support. All adsorption energy values have been corrected to account for the zero-point energy within the harmonic approximation. For the gas phase species, the Gibbs free energy have been computed at 363K and the adsorption energy has been calculated following the eq 1:

$$\Delta G_{for} = G_{H_xRh(CO)_y} - G_{Rh@C_3N_4} - \frac{1}{2} x G_{H_2(363K)} - y G_{CO(363K)}$$

where $G_{H_xRh(CO)_y}$ is the Gibbs energy of the adsorbed cluster, $G_{Rh@C_3N_4}$ is the Gibbs energy of the bare support with the anchored Rh atom, and $G_{H_2(363K)}\ and\ G_{CO(363K)}$ correspond to the Gibbs energy of H_2 and CO molecules at 363K. Note that the Gibbs free energy has been calculated following the approximate procedure proposed by Nørskov et. al,[8] where the entropy of the adsorbed species has been computed. The entropy of gas-phase and adsorbate species is computed with the assumption of rigid rotor and harmonic frequencies.

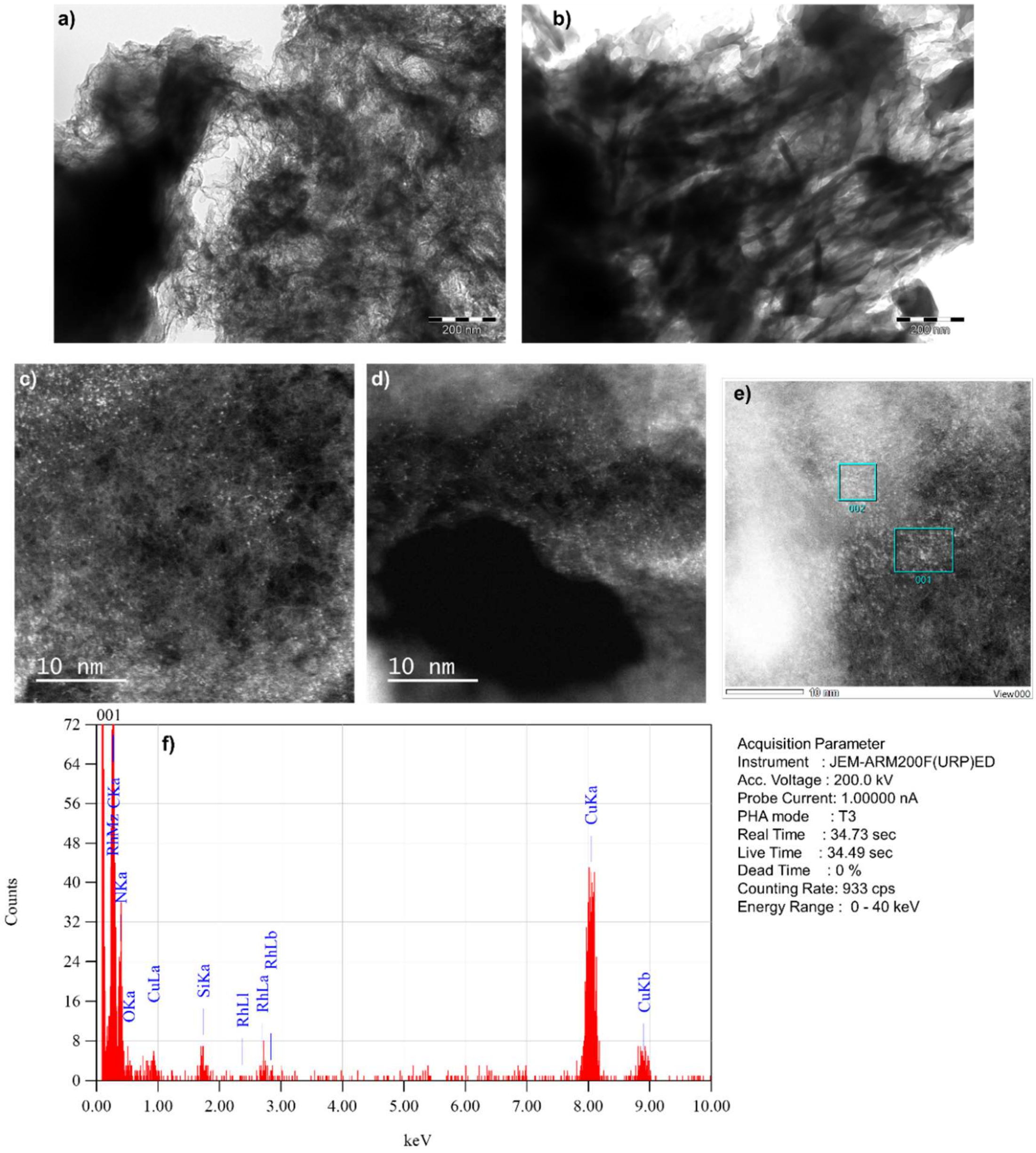

Acquisition Parameter
Instrument : JEM-ARM200F(URP)ED
Acc. Voltage : 200.0 kV
Probe Current: 1.00000 nA
PHA mode : T3
Real Time : 34.73 sec
Live Time : 34.49 sec
Dead Time : 0 %
Counting Rate: 933 cps
Energy Range : 0 - 40 keV

Figure S1. a) and b) TEM, c), d), and e) HAADF-STEM images of Rh/ECN(0.1) (scale bar = 200 and 10 nm, respectively), together with EDX analysis.

Table S1. Rh loading and C, N, H content of the synthesized materials.

	Rh (wt%)[a]	C (at%)[b]	N (at%)[b]	H (at%)[b]	C/N ratio
ECN	-	34	50	14	0.67
Rh/ECN(0.1)	0.10	33	49	15	0.67
Rh-ECN(0.03)	0.03	34	51	10	0.67
Rh-ECN(0.1)	0.10	35	51	9	0.68
Rh-ECN(0.4)	0.37	34	51	10	0.67
Rh-ECN(6.5)	6.50	32	47	10	0.68

[a]From ICP analysis; [b]from elemental analysis

Table S2. Structural and textural properties of the synthesized materials.

	$d_{support}$ (nm)[a]	a (Å)[a]	b (Å)[a]	SSA ($m^2 \cdot g^{-1}$)[b]	V_{pore} ($cm^3 \cdot g^{-1}$)[b]
ECN	3.7	6.615	3.261	5.4	0.04
Rh/ECN(0.1)	3.7	6.660	3.267	5.6	0.03
Rh-ECN(0.03)	4.0	6.660	3.274	6.1	0.05
Rh-ECN(0.1)	4.0	6.586	3.244	5.6	0.03
Rh-ECN(0.4)	4.1	6.626	3.243	6.1	0.04
Rh-ECN(6.5)	-	-	3.263	14.4	0.04

[a]Estimated from XRD analysis; [b]from N_2 physisorption analysis.

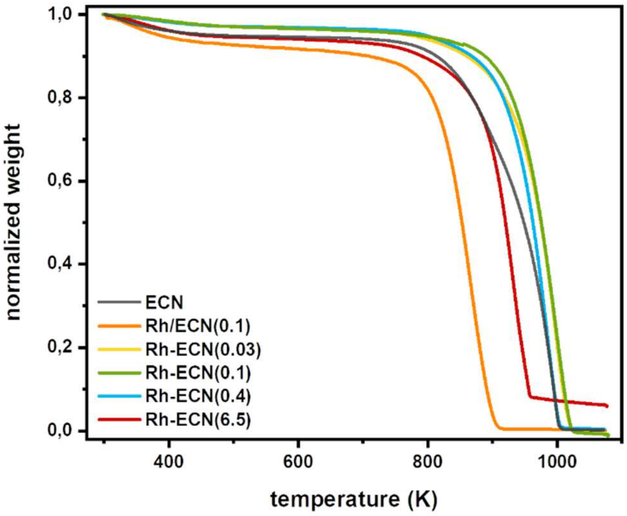

Figure S2. Thermogravimetric analysis curves under N_2 for ECN, Rh/ECN(0.1), Rh-ECN(0.03), Rh-ECN(0.1), Rh-ECN(0.4), and Rh-ECN(6.5).

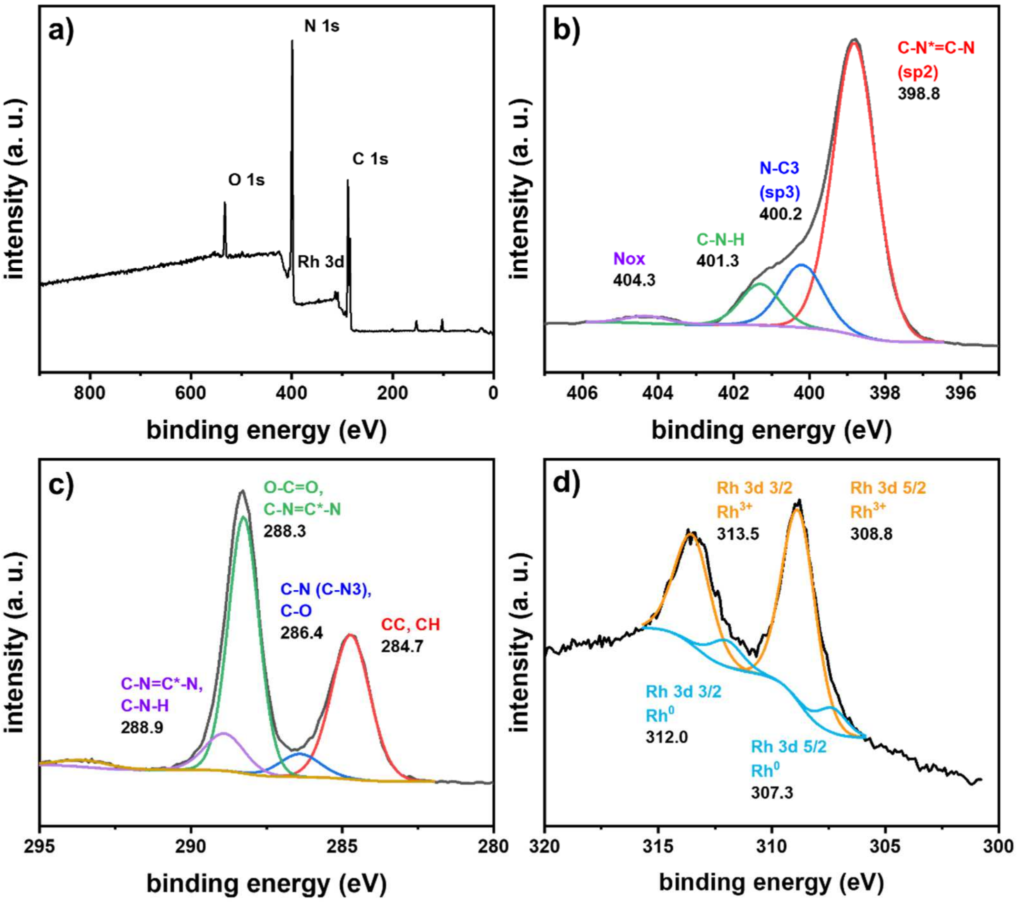

Figure S3. a) XPS survey spectrum of Rh/ECN(0.1); and high-resolution scan spectra of b) N 1s, c) C 1s, and d) Rh 3d.

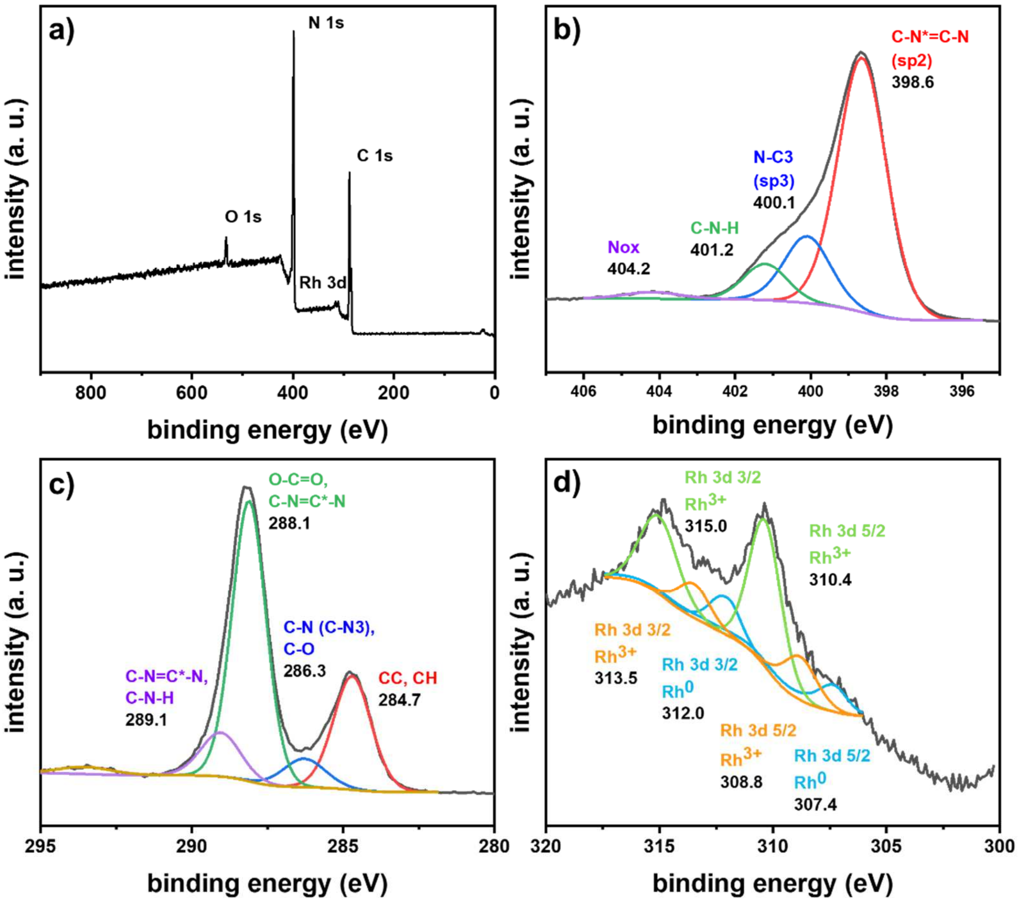

Figure S4. a) XPS survey spectrum of Rh-ECN(0.4); and high-resolution scan spectra of b) N 1s, c) C 1s, and d) Rh 3d.

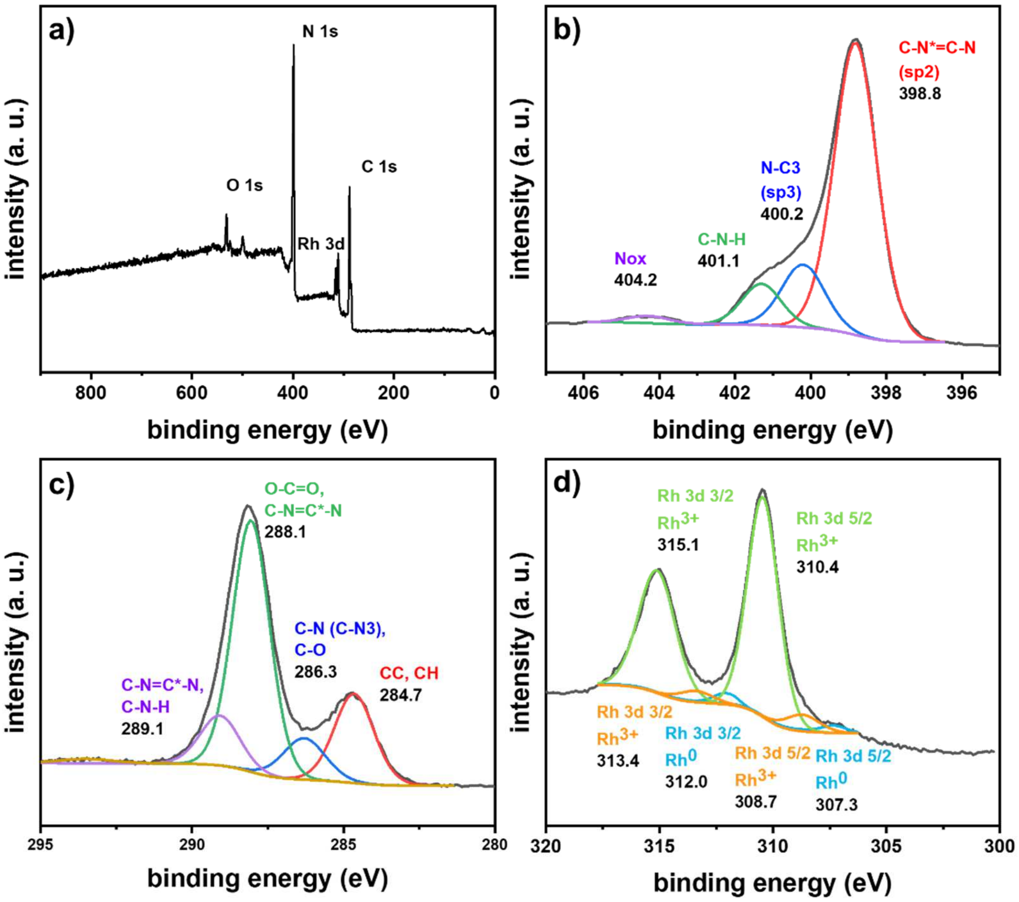

Figure S5. a) XPS survey spectrum of Rh-ECN(6.5); and high-resolution scan spectra of b) N 1s, c) C 1s, and d) Rh 3d.

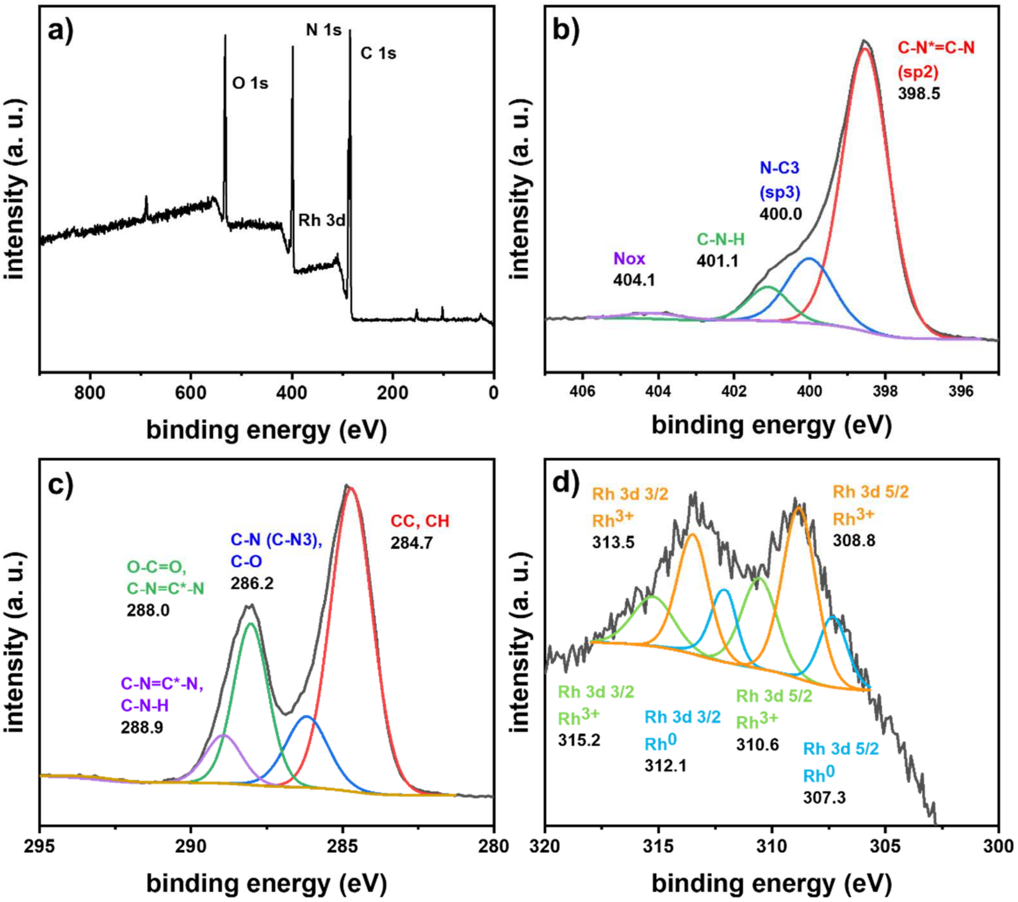

Figure S6. a) XPS survey spectrum of Rh/ECN(0.1) after catalysis; and high-resolution scan spectra of b) N 1s, c) C 1s, and d) Rh 3d.

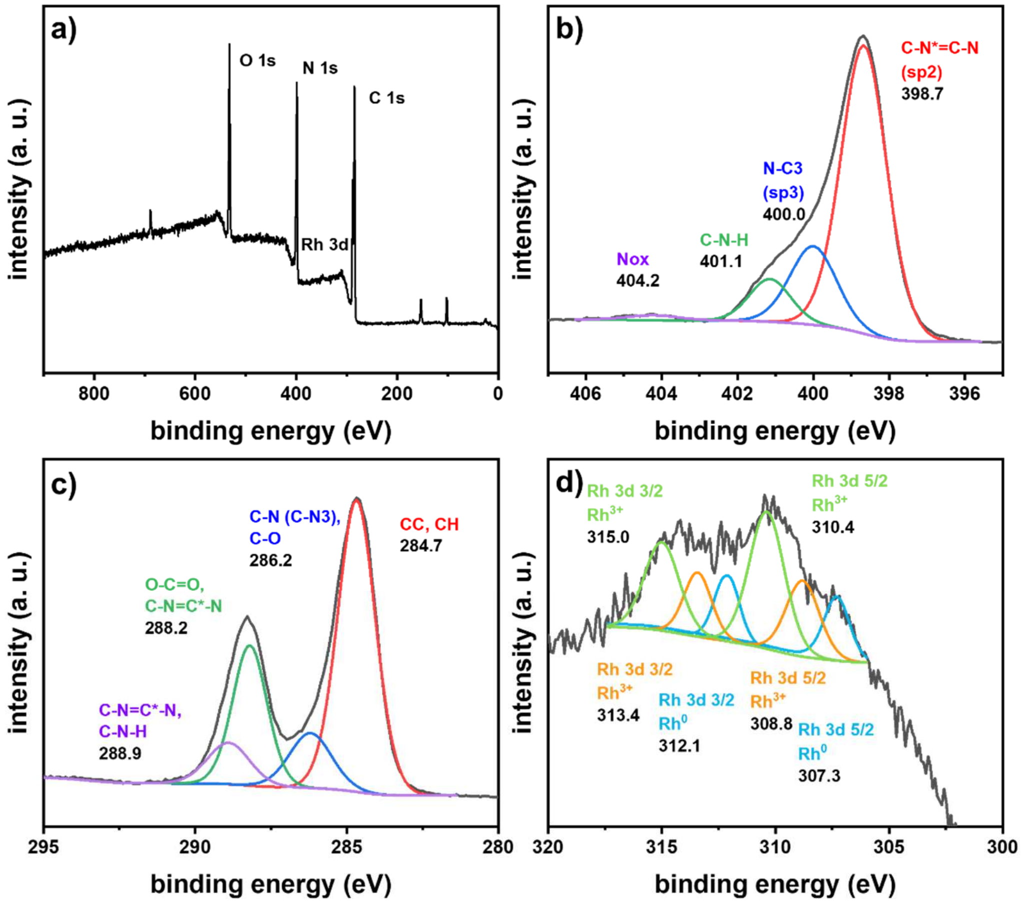

Figure S7. a) XPS survey spectrum of Rh-ECN(0.4) after catalysis; and high-resolution scan spectra of b) N 1s, c) C 1s, and d) Rh 3d.

Table S3. XPS Binding energies and atomic % of Rh SAC before and after catalysis.

	Rh/ECN(0.1)		Rh-ECN(0.4)		Rh-ECN(6.5)		Rh/ECN(0.1) after catalysis		Rh-ECN(0.4) after catalysis	
	Binding energy (eV)	Atomic %	Binding energy (eV)	Atomic %	Binding energy (eV)	Atomic %	Binding energy (eV)	Atomic %	Binding energy (eV)	Atomic %
Rh 3d 5/2 Rh metal	307,3	<0,1	307,4	<0,1	307,3	<0,1	307,3	<0,1	307,3	<0,1
Rh 3d 5/2 Rh^{3+}	308,8	0,2	308,8	<0,1	308,7	0,1	308,8	0,1	308,8	<0,1
Rh 3d 5/2 Rh^{3+}	-	-	310,4	<0,1	310,4	0,7	310,6	<0,1	310,4	<0,1
Rh 3d 3/2 Rh metal	312,0	<0,1	312,0	<0,1	312,0	<0,1	312,1	<0,1	312,1	<0,1
Rh 3d 3/2 Rh^{3+}	313,5	0,1	313,5	<0,1	313,4	<0,1	313,5	<0,1	313,4	<0,1
Rh 3d 3/2 Rh^{3+}	-	-	315,0	<0,1	315,1	0,4	315,2	<0,1	315,0	<0,1
N1s C-N*=C-N (sp2)	398,8	29,5	398,6	33,3	398,6	30,7	398,5	16,0	398,7	16,1
N1s N-C3 (sp3)	400,2	6,4	400,1	8,5	400,0	12,5	400,0	3,7	400,0	4,5
N1s C-N-H	401,3	3,8	401,2	4,3	401,1	4,1	401,1	1,7	401,1	2,2
N1s NOx	404,3	0,7	404,2	1,0	404,2	0,5	404,1	0,4	404,2	0,3
C1s CC, CH	284,7	18,2	284,7	12,1	284,7	9,4	284,7	33,8	284,7	31,5
C1s C-N (C-N3), C-O	286,4	3,1	286,3	3,4	286,3	4,7	286,2	8,0	286,2	6,6
C1s O-C=O, C-N=C*-N	288,3	25,6	288,1	26,9	288,1	25,0	288,0	15,0	288,2	13,9
C1s C-N=C*-N, C-N-H	288,9	4,8	289,1	4,9	289,1	5,3	288,9	4,7	288,9	5,0

Rh coverage on C_3N_4 surface

The Rh atoms can be deposited on the first layer (TOP), on the 6-fold cavity site forming a 6-ring with 2 C and 3 N atoms, or intercalated between the first and second layer (INT). The simulations have been performed on (2×2) surfaces of C_3N_4, containing 24 C atoms C and 32 N atoms . Different Rh coverages have been investigated on both surface sites and the results are listed in Table S4.

Table S4. Relative energies (eV) of Rh adsorption at different coverages (Θ_{Rh}) on TOP and INT sites. The Θ_{Rh} considers the number of Rh *per* C atoms on the most exposed layer.

Θ_{Rh} (Rh/C)	$E_{rel/Rh\ atom}$ TOP (eV)	$E_{rel/Rh\ atom}$ INT (eV)
1/6	0.57	0.00
1/8	0.39	0.00
1/12	0.30	0.00
1/24	0.00	0.75

At high coverage (Rh/C 1/6) the Rh atoms are stably adsorbed between C_3N_4 layers, *i.e.* the INT site. Decreasing the Rh coverage reduces the energy difference between both adsorption sites until TOP adsorption is more favored (Rh/C 1/24).

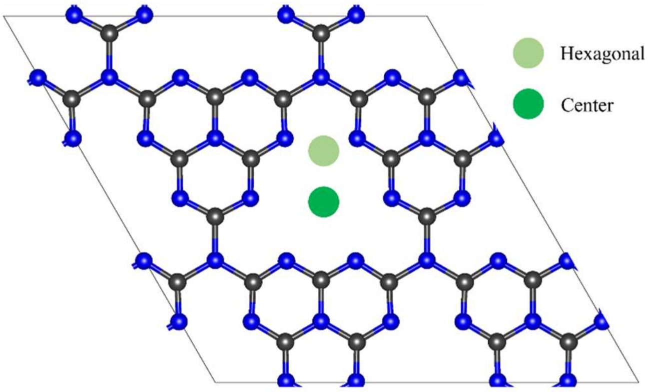

Figure S8. Rh adsorption on C_3N_4: tested sites: hexagonal 1st layer, hexagonal 2nd layer, center 1st layer, center 2nd layer, top N, top C, and between layers.

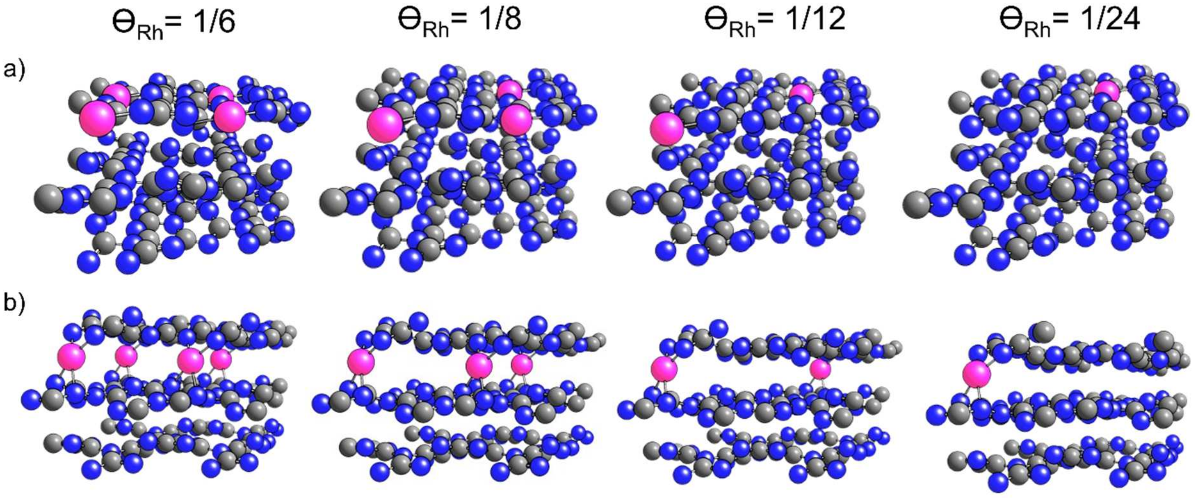

Figure S9. Rh atoms deposited a) on the first layer (TOP) of ECN and b) intercalated between the first and second layer (INT).

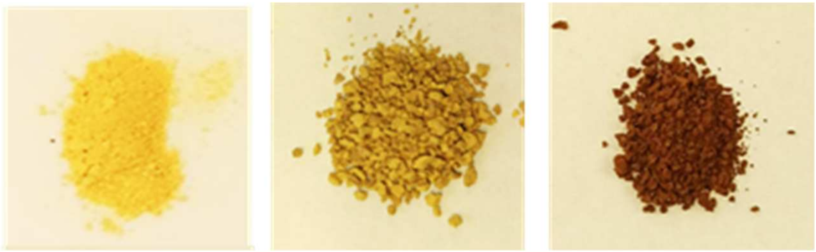

Figure S10. Images of a) ECN; b) Rh/ECN(0.1); c) Rh-ECN(0.4); and Rh-ECN(6.5).

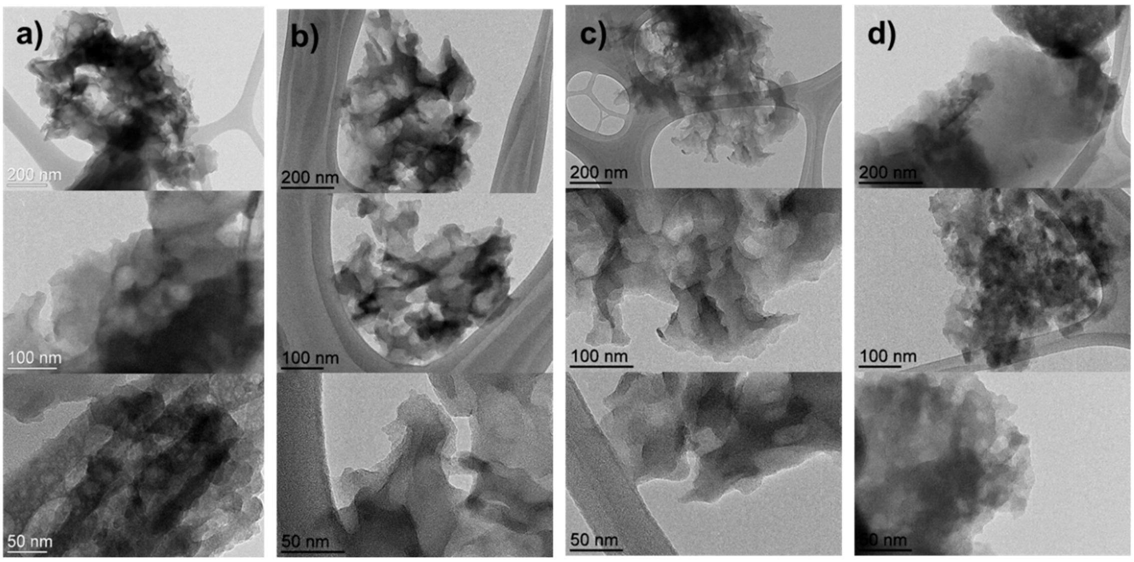

Figure S11. TEM images of a) Rh/ECN(0.03); b) Rh/ECN(0.1); c) Rh-ECN(0.4); and d) Rh-ECN(6.5). (scale bar = 200, 100 and 50 nm, respectively).

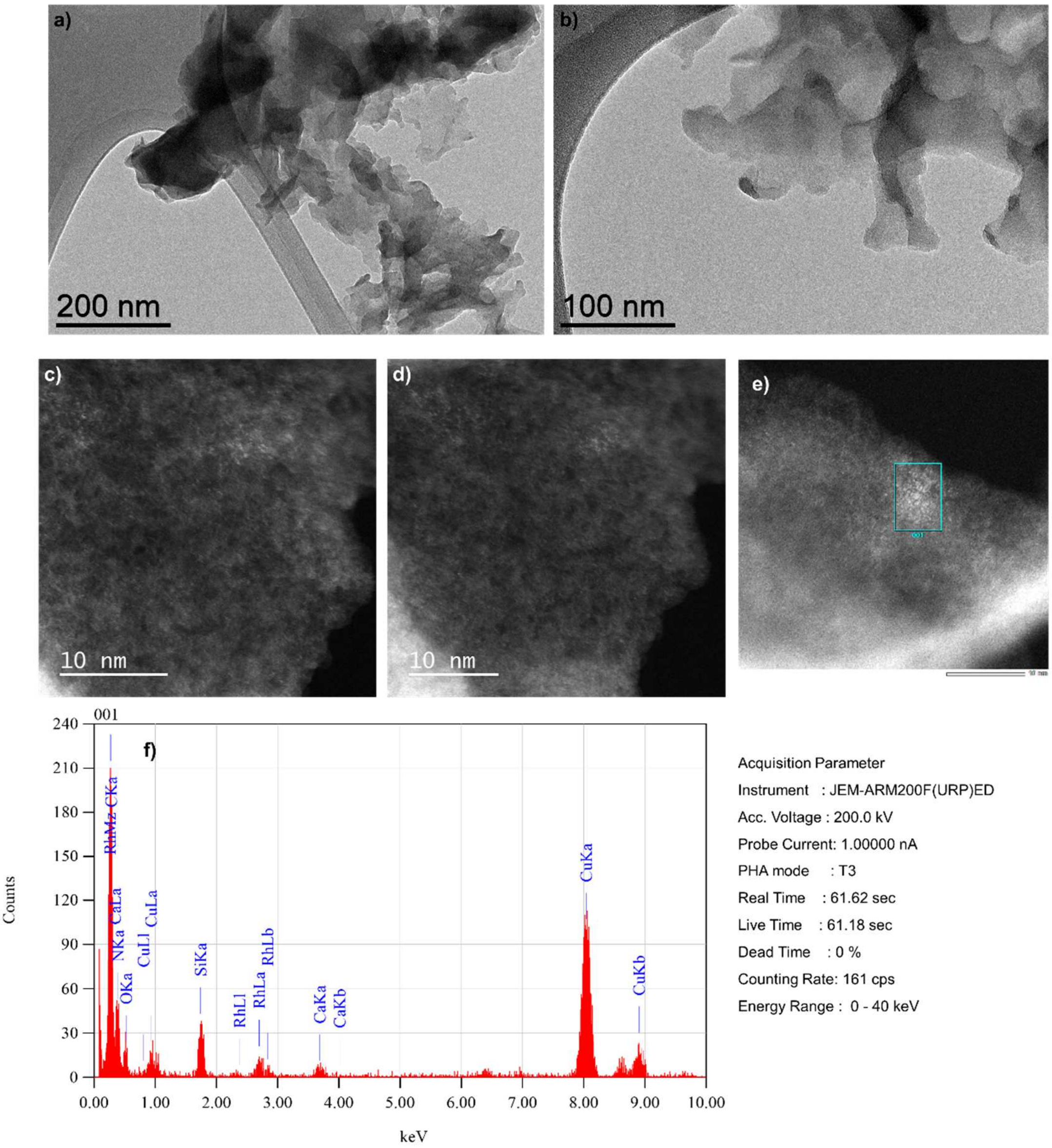

Acquisition Parameter
Instrument : JEM-ARM200F(URP)ED
Acc. Voltage : 200.0 kV
Probe Current: 1.00000 nA
PHA mode : T3
Real Time : 61.62 sec
Live Time : 61.18 sec
Dead Time : 0 %
Counting Rate: 161 cps
Energy Range : 0 - 40 keV

Figure S12. a) and b) TEM, c), d), and e) HAADF-STEM images of Rh-ECN(0.4) (scale bar = 200 and 10 nm, respectively), together with the EDX analysis.

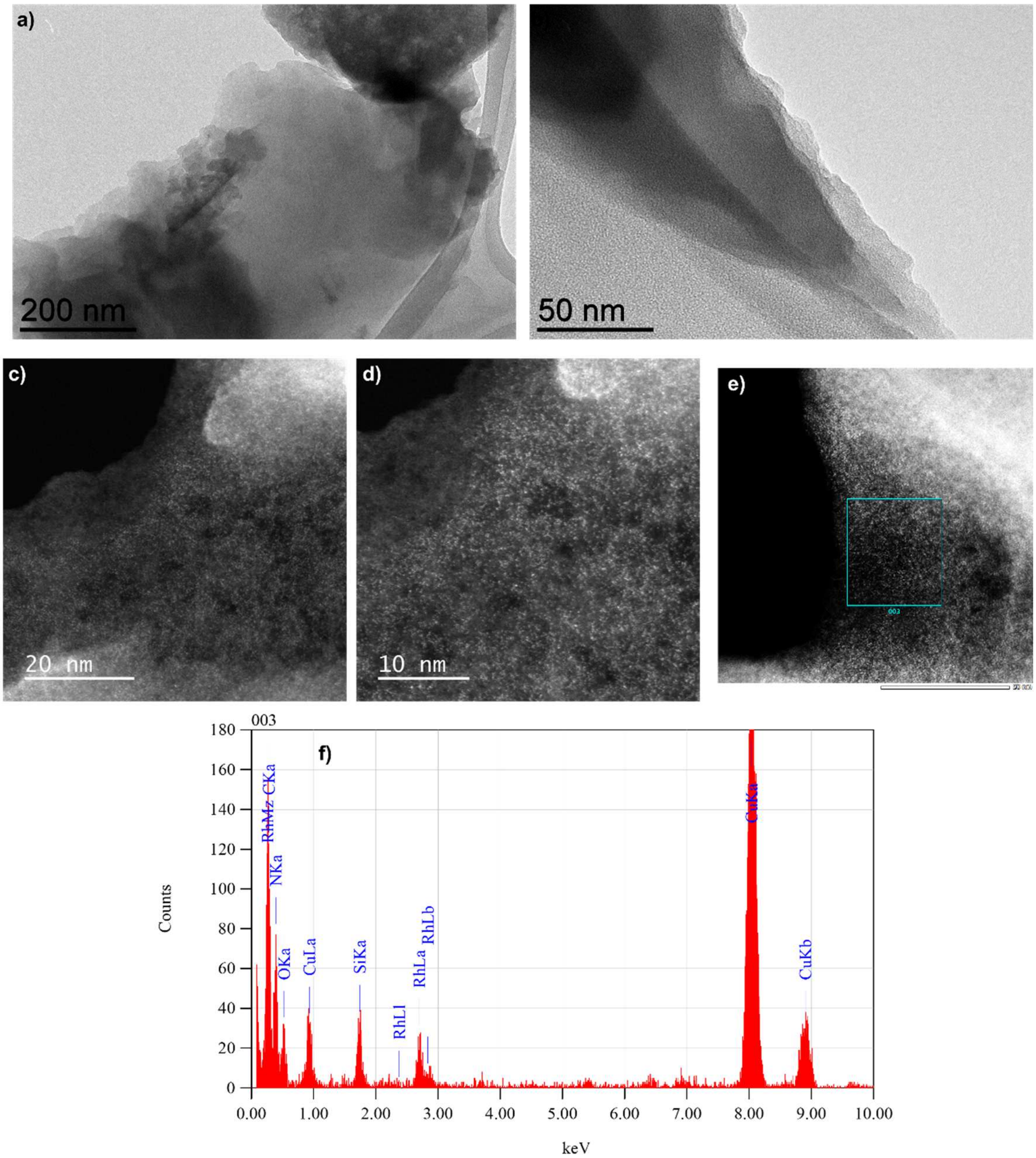

Figure S13. a) and b) TEM, c), d), and e) HAADF-STEM images of Rh-ECN(6.5) (scale bar = 200, 50, 20 and 10 nm, respectively), together with the EDX analysis.

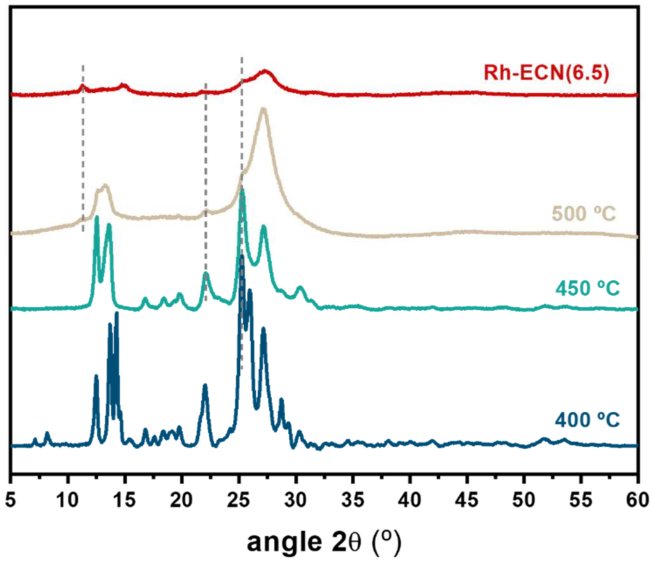

Figure S14. XRD difractograms of dicyandiamide at several pyrolyzing temperatures together with Rh-ECN(6.5).

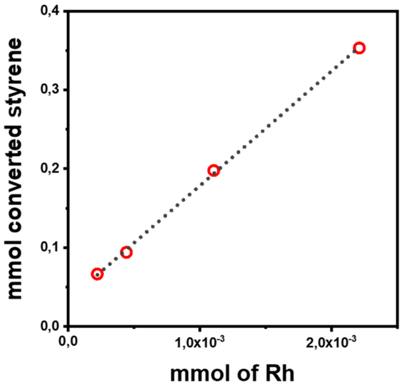

Figure S15. Conversion of styrene (mmol) vs. amount of [Rh(η^3-C_3H_5)$_3$] precatalyst (mmol). Reaction conditions: 0.04, 0.09, 0.22, or 0.44 mM of Rh, 1 mmol of styrene, 0.25 mmol of octane (internal standard), 20 bar of syngas (CO/H_2 = 1), 5 mL of THF, 5h, 343 K, 1200rpm.

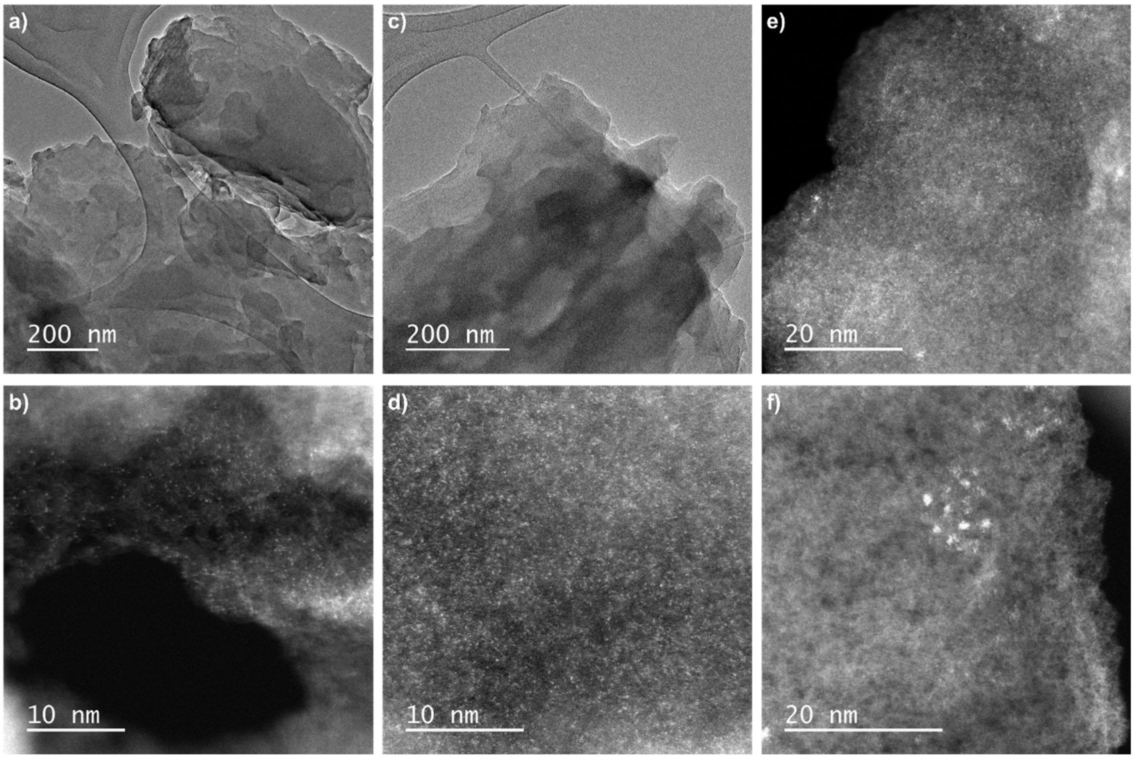

Figure S16. HRTEM and HAADF-STEM images of a) and b) Rh/ECN(0.1) after catalysis: c) and d) Rh-ECN(0.4) after catalysis; and e) and f) Rh/ECN(0.1) after four catalytic runs (scale bar = 200, 10, 200, 10 and 20 nm, respectively).

Table S5. Assignation of the bands extracted from DFT calculations

Species	Vibration frequencies (cm^{-1})		
Rh(CO)	1986		
Rh(CO)$_2$	2056 (symmetric)[a]	1997 (asymmetric)[b]	
Rh(CO)$_3$[c]	2054 (symmetric)	2001 (asymmetric)	1997(asymmetric)
Rh(CO)$_2$ + *CO[d]	2082 (CO physiosorbed)	2057 (symmetric)	2001 (asymmetric)

[a]Symmetric: The CO stretching is the same, the vibration is equally for both CO.

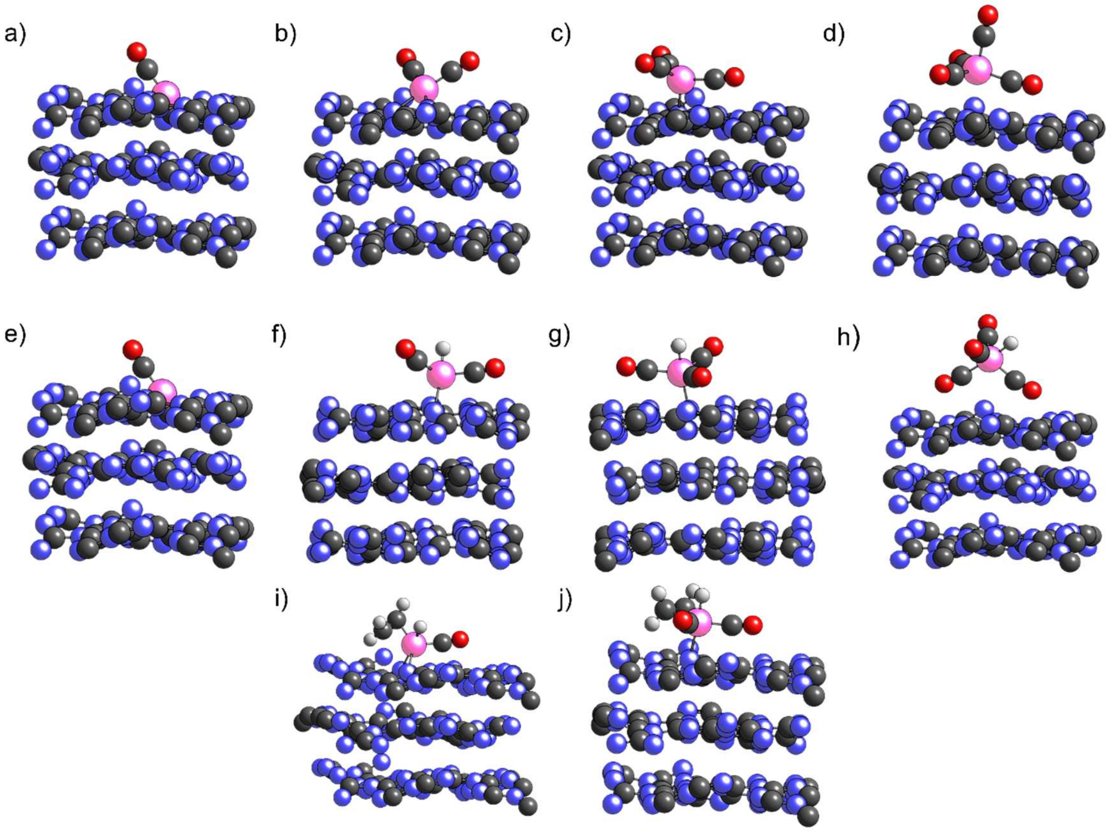

Figure S17: Sketches of a) Rh(CO)$_1$, b) Rh(CO)$_2$, c) Rh(CO)$_3$, d) Rh(CO)$_4$, e) H$_1$Rh(CO)$_1$, f) H$_1$Rh(CO)$_2$, g) H$_1$Rh(CO)$_3$, h) H$_1$Rh(CO)$_4$, i) H$_1$Rh(CO)(C$_2$H$_4$) and j) H$_1$Rh(CO)$_2$(C$_2$H$_4$) supported on ECN (grey, blue, pink, red, and white balls represent carbon, nitrogen, rhodium, oxygen, and hydrogen atoms respectively).

References

[1] G. Kresse, J. Furthmüller, Efficient iterative schemes for *ab initio* total-energy calculations using a plane-wave basis set, Phys. Rev. B, 54 (1996) 11169-11186.

[2] J.P. Perdew, K. Burke, M. Ernzerhof, Generalized gradient approximation made simple, Phys. Rev. Lett., 77 (1996) 3865-3868.

[3] S. Grimme, J. Antony, S. Ehrlich, H. Krieg, A consistent and accurate ab initio parametrization of density functional dispersion correction (DFT-D) for the 94 elements H-Pu, J. Chem. Phys., 132 (2010) 154104/154101-154104/154119.

[4] P.E. Blöchl, Projector augmented-wave method, Phys. Rev. B, 50 (1994) 17953-17979.

[5] G. Kresse, D. Joubert, From ultrasoft pseudopotentials to the projector augmented-wave method, Phys. Rev. B, 59 (1999) 1758-1775.

[6] H.J. Monkhorst, J.D. Pack, Special points for Brillouin-zone integrations., Phys. Rev. B, 13 (1976) 5188-5192.

[7] S.P. Ong, W.D. Richards, A. Jain, G. Hautier, M. Kocher, S. Cholia, D. Gunter, V.L. Chevrier, K.A. Persson, G. Ceder, Python Materials Genomics (pymatgen): a robust, open-source python library for materials analysis, Comput. Mater. Sci., 68 (2013) 314-319.

[8] J.K. Nørskov , F. Studt, F. Abild-Pedersen, T. Bligaard, Fundamental concepts in heterogeneous catalysis, Catalysis Wiley, New Jersey, 2014.